ARTICLE

Journal of Materials Chemistry
www.rsc.org/materials

Biological synthesis of metal carbonate minerals using fungi and actinomycetes

Debabrata Rautaray,[a] Absar Ahmad[b] and Murali Sastry*[a]

[a]*Materials Chemistry Division, National Chemical Laboratory, Pune-411008, INDIA. E-mail: sastry@ems.ncl.res.in; Fax: +91 20 25893952/25893044; Tel: +91 20 25893044*
[b]*Biochemical Sciences Division, National Chemical Laboratory, Pune-411008, INDIA*

Received 29th January 2004, Accepted 8th March 2004
First published as an Advance Article on the web 31st March 2004

The exciting possibility of biosynthesis of minerals of variable morphology and with polymorph selectivity by challenging microorganisms such as fungi and actinomycetes has been described. Many fungi and actinomycetes are known to produce reasonable amounts of CO_2 during growth. We show here that CO_2 and characteristic proteins released from an endophytic fungus, *Verticillium* sp. and an extremophilic actinomycete, *Thermomonospora* sp. may be reacted with aqueous Ca^{2+} and Ba^{2+} ions to produce truly biogenic $CaCO_3$ and $BaCO_3$ crystals. While extracellular synthesis of the highly unstable vaterite polymorph of $CaCO_3$ in a spherical morphology was observed with the fungus, both extra- and intracellular formation of $CaCO_3$ in the form of composites of flat plates and branched elongated flat plates, were observed with the actinomycete. Reaction of Ba^{2+} ions with *Verticillium* sp. and *Thermomonospora* sp. resulted in the extracellular synthesis of $BaCO_3$ crystals of spherical and flat, plate-like morphologies respectively. The action of specific proteins secreted by the microorganisms in directing crystal structure and morphology has been addressed.

Introduction

Natural organisms are capable of generating crystalline materials with complex morphologies at ambient temperature in water by the process of biomineralization. The biomineralization process occurs in many different species and tissues, including bone mineral, tooth enamel and marine shells. Many of the mineralized tissues formed by organisms are functional and have advantageous mechanical properties. In biological systems, almost all mineralized tissues consist of a distinctive assemblage of acidic proteins, glycoproteins and polysaccharides and it is widely accepted that these highly anionic, soluble biomacromolecules, play an important role in biomineralization and act as nucleators, growth modifiers, and anchoring units in the mineral formation.[1] Apart from controlling their nucleation and growth into specific sizes and shapes, these biomacromolecules also exert exquisite control over the polymorphism of a particular mineral phase.[1,2]

Biological systems provide a number of examples of inorganic materials in both unicellular and multicellular organisms synthesized either intra- or extracellularly.[3,4] Some well-known examples of bio-organisms synthesizing inorganic materials include magnetotactic bacteria (which synthesize magnetite nanoparticles),[5–7] diatoms (which synthesize siliceous materials),[8–10] and S-layer bacteria (which produce gypsum and calcium carbonate layers).[11,12] The secrets gleaned from nature have lead to the development of biomimetic approaches for the growth of advanced inorganic materials.

The biomimetic laboratory synthesis of metal carbonates, especially calcium carbonate ($CaCO_3$), has been studied in great detail due to their abundance in nature and also their important industrial application in the paint, plastics, rubber and paper industries. $CaCO_3$ has three known polymorphs: calcite, aragonite and vaterite. Calcite is thermodynamically the most stable polymorph, aragonite is slightly less stable than calcite, whereas vaterite is the most unstable polymorph. Calcite and aragonite are often found in biominerals, whereas the metastable polymorph vaterite is not often seen in biological systems.[13,14] The three polymorphs have markedly different physicochemical characteristics, and it is often found that the less stable forms are stabilized kinetically and/or biochemically.

Elucidation of general biomineralization principles has followed from studies into the growth of minerals in biological organisms[1,15] and on biomacromolecules extracted from organisms.[16] The important biomineral $CaCO_3$ has received considerable attention and these principles have been used in the development of a number of biomimetic templates such as Langmuir monolayers,[17–21] dynamic liquid–liquid interfaces,[22] self-assembled monolayers,[23] lipid bilayer stacks,[24] vesicles[25] and functionalized micro-patterned surfaces[26] for its synthesis. Morphology variation and polymorph selectivity of $CaCO_3$ crystals have also been achieved by growth in solution in the presence of suitably designed additives such as proteins extracted from $CaCO_3$-rich organisms[16] or synthetic molecules such as polymers.[27–28]

Barium carbonate ($BaCO_3$) is another important mineral that exists in nature as a thermodynamically more stable crystal modification among the heavy metal carbonates. $BaCO_3$ has also attracted attention due to its close relationship with aragonite and many important applications in the ceramic and glass industries. It is also a highly utilized precursor in the synthesis of magnetic ferrites and ferroelectric materials.[29] Related biomimetic approaches for $BaCO_3$ crystallization include influence of urease,[30] presence of polyelectrolytes,[29] and double hydrophilic block copolymers[31] as crystal modifiers.

As discussed above, laboratory processes for the synthesis of metal carbonate minerals have mostly relied on an external source of CO_2 for reaction with desired metal cations in the presence of synthetic molecules or very specific proteins from mineral producing organisms to achieve polymorph and morphology control. Many fungi and actinomycetes are known to produce reasonable amounts of CO_2 during growth.[32] We show in this paper that CO_2 and characteristic proteins released from a fungus, *Verticillium* sp. and an actinomycete, *Thermomonospora* sp. may be reacted with aqueous Ca^{2+} and Ba^{2+} ions to produce truly biogenic

DOI: 10.1039/b401431f

$CaCO_3$ and $BaCO_3$ crystals. Very recently we have shown that biogenic $CaCO_3$ crystals of complex morphology may be grown by simple exposure of aqueous Ca^{2+} ions to a fungus, *Fusarium* sp. and an actinomycete, *Rhodococcus* sp.[33] and this report represents an important advance in developing this strategy to encompass other microorganisms and mineral compositions. While extracellular synthesis of the highly unstable vaterite polymorph of $CaCO_3$ in a spherical morphology is obtained with *Verticillium* sp., both extra- and intra-cellular formation of $CaCO_3$ in the form of flat plates and branched elongated flat plates was observed with *Thermomonospora* sp. Extracellular synthesis of $BaCO_3$ crystals of spherical morphology and flat plate assemblies were observed using *Verticillium* sp. and *Thermomonospora* sp. respectively. Significant differences in the morphology and polymorph selectivity of the minerals were observed indicating that the proteins secreted by the fungus and the actinomycete play crucial roles in stabilizing and directing the crystal growth. The interesting morphology variation and polymorph selectivity during the mineralization process, as a result of proteins secreted by organisms such as fungi and actinomycetes, which are not normally (if ever) exposed to such metal ions, is an exciting outcome and underlines the untapped potential of biological methods in expanding the scope of crystal engineering. Presented below are the details of this study.

Experimental

In typical experiments, an endophytic fungus, *Verticillium* sp. (isolated from the *Taxus* plant) and an extremophilic actinomycete, *Thermomonospora* sp. (isolated from self-heating compost) were maintained on potato-dextrose-agar (PDA) slants. Stock cultures were maintained by sub culturing at monthly intervals. After growing at pH 7 and 27 °C (pH 9 and 50 °C for *Thermomonospora* sp.) for four days, the slants were preserved at 15 °C. From actively growing stock cultures, subcultures of both the fungus and actinomycete were made on fresh slants and after four days of incubation at pH 7 and 27 °C, were used as the starting materials for fermentation experiments. For the synthesis of $CaCO_3$ and $BaCO_3$ crystals both the fungus and actinomycete were grown in 500 ml Erlenmeyer flasks containing 100 ml malt extract-glucose-yeast extract-peptone (MGYP) medium which is composed of malt extract (0.3%), glucose (1%), yeast extract (0.3%) and peptone (0.5%). After adjusting the pH of the medium to 7, the cultures were grown under continuous shaking on a rotary shaker (200 rpm) at 27 °C for 96 hours. After 96 hours of fermentation, mycelia of the fungus and the actinomycete were separated from the culture broth by centrifugation (5000 rpm) at 20 °C for 20 minutes and then the mycelia were washed thoroughly with sterile distilled water under sterile conditions. The harvested mycelial mass (20 g wet wt. of mycelia) of *Verticillium* sp. and *Thermomonospora* sp. was then resuspended in 100 ml of 10^{-3} M $CaCl_2$ and $BaCl_2$ solutions in 500 ml Erlenmeyer flasks separately. These flasks were then put into a shaker at 27 °C (200 rpm) and the reaction carried out for a period of 72 hours. The biotransformation of Ca^{2+} and Ba^{2+} ions into $CaCO_3$ and $BaCO_3$ respectively was monitored by separating the fungal and actinomycete mycelia from the respective reaction media by filtration, and subjecting both the filtrate and mycelia to analysis as described below. That formation of the minerals had occurred could be inferred from the fact that the filtrate became turbid and milky white after roughly 2 days of reaction. pH values of 5.3 and 6.2 were recorded from the reaction medium after 3 days of reaction of Ca^{2+} ions with *Verticillium* sp. and *Thermomonospora* sp. respectively. The residues after 3 days of reaction were washed thoroughly several times using copious amounts of double distilled water and the washed biomass was cast in the form of films onto different solid supports. The filtrates were subjected to centrifugation at 10000 rpm and the pellets obtained were washed repeatedly with copious amounts of double distilled water. The purified pellets were solution-cast in the form of films onto different solid supports for further analysis. Please note that considerable care was taken to wash the $CaCO_3$ and $BaCO_3$ crystals synthesized using fungus and actinomycetes, prior to analysis. This precaution was taken to remove uncoordinated proteins in the reaction medium from the biogenic $CaCO_3$ and $BaCO_3$ crystals. These films were then characterized by Fourier transform infrared spectroscopy (FTIR), X-ray diffraction (XRD), scanning electron microscopy (SEM) and energy dispersive analysis of X-rays (EDAX). FTIR spectroscopy measurements of the purified and dried biogenic $CaCO_3$ and $BaCO_3$ powders taken in KBr pellets were carried out on a Perkin-Elmer Spectrum-One instrument at a resolution of 2 cm^{-1}. XRD measurements of solution-cast films of the biogenic $CaCO_3$ and $BaCO_3$ crystals on glass substrates were carried out on a Phillips PW 1830 instrument operated at a voltage of 40 kV and a current of 30 mA with Cu K_α radiation. For SEM analysis, solution-cast films of biogenic $CaCO_3$ and $BaCO_3$ crystals were made on Si (111) substrates. SEM measurements were performed on a Leica Stereoscan-440 instrument equipped with a Phoenix energy dispersive analysis of X-rays (EDAX) attachment. Please note that the mass of materials used in the FTIR and XRD analysis were 2 mg and 10 mg respectively to obtain acceptable signal to noise ratios.

Control experiments were performed wherein the biomass of the fungus, *Verticillium* sp. and the actinomycete, *Thermomonospora* sp. were soaked in water for 3 days. The aqueous component with secreted proteins was separated by filtration and $CaCl_2$ and $BaCl_2$ were added to the filtrates separately to attain a concentration of 10^{-3} M of the metal cation. CO_2 was bubbled very slowly through these solutions and the $CaCO_3$ and $BaCO_3$ crystals formed were washed thoroughly and were analyzed by FTIR, XRD, SEM and EDAX.

Control experiments were also performed to understand whether repeated washing of the biogenic $CaCO_3$ crystals synthesized using *Verticillium* sp. and *Thermomonospora* sp. results in the partial dissolution of the crystals or surface rearrangement in the minerals. The biogenic $CaCO_3$ crystals filtered from the respective culture media without any washing were vacuum dried to a powder and analyzed by FTIR and SEM. In order to realize the presence of proteins in the biogenic $CaCO_3$ crystals synthesized using *Verticillium* sp. and *Thermomonospora* sp., the aqueous solutions containing biogenic $CaCO_3$ crystals were treated with 4% sodium hypochlorite (NaOCl) solution. Thereafter, the solutions containing NaOCl treated biogenic $CaCO_3$ crystals were subjected to centrifugation and the pellets obtained were washed with copious amounts of double distilled water. The purified pellets were dried and analyzed by FTIR and SEM.

Results and discussion

Figs. 1A & B show representative SEM images recorded from solution-cast films of the aqueous $CaCl_2$ solution after reaction with *Verticillium* sp. for 3 days. After 3 days of reaction, the formation of very uniform $CaCO_3$ nanocrystallites was observed (Fig. 1A). The size of the crystallites determined from the SEM image was in the range 70–100 nm. The higher magnification SEM image clearly shows that the $CaCO_3$ crystallites are circular in shape with some evidence of their being flat (Fig. 1B). One of the circular $CaCO_3$ crystals is shown in the inset of Fig. 1B. Such spherical/circular morphology of $CaCO_3$ crystals is indicative of the formation of the highly unstable vaterite polymorph.[16] The FTIR spectrum recorded from the circular $CaCO_3$ crystals synthesized using *Verticillium* sp. is shown in Fig. 2A, curve 1. The

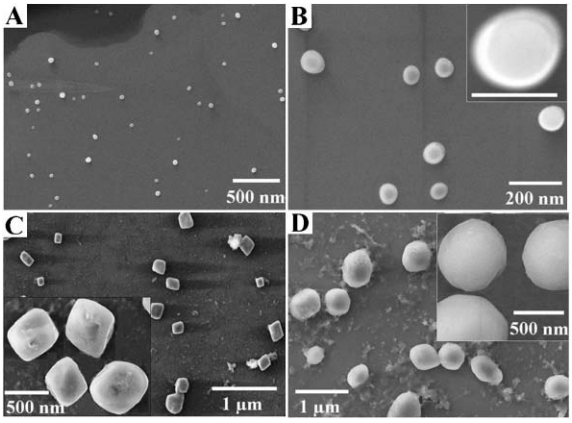

Fig. 1 (A and B) Representative SEM micrographs of $CaCO_3$ crystals grown after 3 days of reaction of aqueous Ca^{2+} ions with *Verticillium* sp. The inset in B shows a magnified view of one of the flat, circular $CaCO_3$ crystals (scale bar = 100 nm). (C) SEM micrograph of $CaCO_3$ crystals (shown in A & B) after calcination at 300 °C for 3 h. The inset shows a magnified view of the faceted $CaCO_3$ crystals obtained in the main figure. (D) SEM micrograph of $CaCO_3$ crystals grown using extract from *Verticillium* sp. (see text for details).

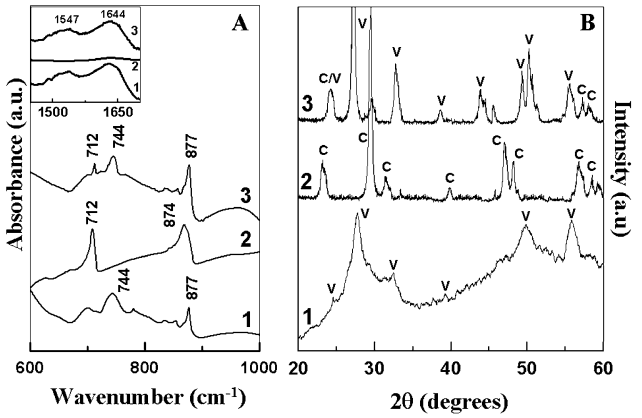

Fig. 2 (A and inset) FTIR spectra in different spectral windows recorded from: $CaCO_3$ crystals obtained by the reaction of aqueous Ca^{2+} ions for 3 days with the fungus *Verticillium* sp. before (curve 1) and after calcination at 300 °C for 3 h (curve 2) and $CaCO_3$ crystals grown using extract from *Verticillium* sp. (curve 3). (B) XRD patterns recorded from solution-cast films of $CaCO_3$ crystals synthesized using *Verticillium* sp. on glass substrate before (curve 1) and after calcination at 300 °C for 3 h (curve 2). Curve 3 corresponds to the XRD pattern recorded from a solution-cast film of $CaCO_3$ crystals grown using extract from *Verticillium* sp. (curve 3). In the XRD spectra, 'V' stands for vaterite and 'C' for calcite (see text for details).

absorption bands at 744 and 877 cm^{-1} are characteristic of vaterite.[16] XRD analysis of the $CaCO_3$ crystallites formed by the reaction of aqueous Ca^{2+} ions with *Verticillium* sp. for 3 days was performed and the pattern obtained is shown as curve 1 in Fig. 2B. The Bragg reflections identified by 'V' agree excellently with those reported for vaterite.[34] The broad Bragg reflections in the XRD spectrum are clearly indicative of small crystallites in agreement with the SEM results (Figs. 1A & B). Studies on the synthesis of spherical vaterite crystals are relatively scarce with the synthesis having been achieved in the presence of divalent cations,[35] using AOT microemulsions,[36] and poly(vinyl) alcohol[37]/double hydrophilic block copolymers as additives.[38,39] Control over the size of spherical vaterite crystals would be important in application of the minerals as pigments, fillers, and in cosmetics/pharmaceutical formulations. Vaterite is thermodynamically the most unstable polymorph of the three crystal structures of $CaCO_3$ and is used for specific applications requiring high specific surface area, high solubility, high dispersion, and smaller specific

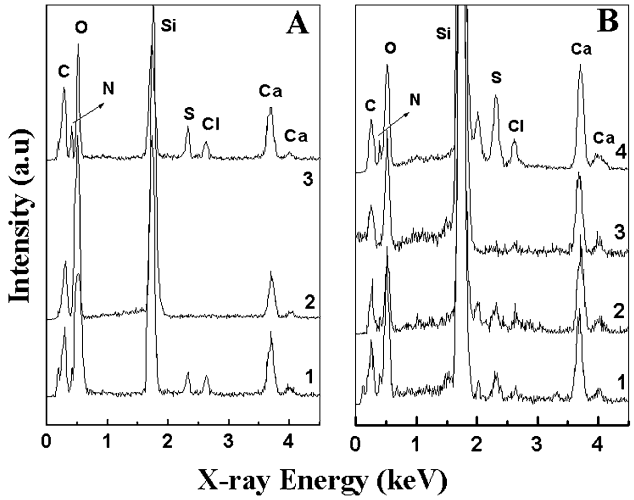

Fig. 3 (A) Spot-profile EDAX spectra recorded from films of $CaCO_3$ crystals synthesized using *Verticillium* sp. before (curve 1) and after calcination at 300 °C for 3 h (curve 2). Curve 3 corresponds to the EDAX spectrum recorded from $CaCO_3$ crystals grown using extracts of *Verticillium* sp. (B) Spot-profile EDAX spectra recorded from the films of $CaCO_3$ crystals synthesized extracellularly (curve 1) and intracellularly (curve 2) using *Thermomonospora* sp., the extracellularly synthesized $CaCO_3$ sample after calcination at 300 °C for 3 h (curve 3). The EDAX spectrum recorded from $CaCO_3$ crystals grown using extracts from *Thermomonospora* sp. (curve 4).

gravity.[40] As mentioned in the experimental section, the pH of the Ca^{2+} – *Verticillium* sp. reaction medium 3 days after reaction was measured to be 5.3. It is known that synthesis of vaterite is facilitated by low pH conditions[31] – clearly, the synthesis of vaterite by *Verticillium* sp. is not due to pH effects and is due to specific proteins secreted by the microorganism.

It would be instructive to understand the chemical composition of the vaterite crystallites synthesized using *Verticillium* sp. This is conveniently done by spot-profile EDAX measurement of one of the circular vaterite crystals grown using the fungus (curve 1, Fig. 3A). In addition to the expected Ca, C and O signals, we observe the presence of N and S signals in the vaterite crystals. This indicates the presence of proteins within the circular vaterite crystallites. That these signals are likely to be due to proteins secreted by the fungus is supported by the FTIR measurement of the vaterite crystals (inset of Fig. 2A, curve 1), which clearly shows the presence of amide II and I bands at 1547 and 1644 cm^{-1} respectively. This observation indicates that the vaterite crystals in the spherical/circular morphology are present with proteins that are possibly occluded into the crystals or are bound to the surface of the crystals. It is clear that specific (and as yet unidentified) proteins secreted by the microorganism play a crucial role in defining the morphology and indeed, crystal structure of the $CaCO_3$ crystals formed. While the exact nature of binding of the proteins with specific crystallographic faces needs elaboration, the location of the proteins in the crystals (surface adsorption *vs.* uniform intercalation in the crystals) may be indirectly determined by removal of the proteins by calcination. Fig. 1C shows an SEM image of biogenic vaterite crystals grown using *Verticillium* sp. after heating at 300 °C for 3 h. Upon calcination, the original spherical/circular crystals are transformed into more faceted crystals. The inset of Fig. 1C shows a magnified view of the faceted crystals which show an increase in the surface roughness suggesting removal of proteins occluded into the crystalline framework on heating. The morphology change from circular to polyhedral suggests a concomitant variation in the crystal structure upon heat treatment, which was ascertained by FTIR and XRD measurement of the calcined samples. The FTIR spectrum of the calcined *Verticillium* sp.-biogenic $CaCO_3$ crystals exhibited

absorption bands at 712 and 874 cm^{-1} (curve 2, Fig. 2A) clearly showing that the calcination-induced morphology variation seen in the SEM images is due to transformation of vaterite into calcite.[41] The XRD pattern recorded from the calcined crystals shows the presence of Bragg reflections characteristic of calcite (peaks marked 'C' in curve 2, Fig. 2B) thus supporting the phase transformation inferred from the FTIR results. The spot-profile EDAX spectrum recorded from the biogenic vaterite crystals after calcination at 300 °C for 3 h is shown as curve 2 in Fig. 3A. As expected, strong Ca, C and O signals are observed but this is accompanied by complete disappearance of N and S signals from the $CaCO_3$ crystals indicating removal of the occluded proteins. The complete disappearance of N and S signals after calcination is also observed in the FTIR spectrum (curve 2 in the inset of Fig. 2A), which clearly shows the absence of the amide bands in the crystals after calcination. Vaterite is the least stable of the polymorphs of $CaCO_3$ and the room temperature synthesis of vaterite by *Verticillium* sp. is a salient feature of this work.

A control experiment was performed wherein the *Verticillium* sp. biomass was immersed in water for 3 days and the aqueous component separated by filtration. The aqueous fraction was taken up with 10^{-3} M $CaCl_2$ and CO_2 was bubbled very slowly through this solution. The $CaCO_3$ crystals formed in this manner were analyzed by SEM, EDAX, FTIR and XRD. SEM analysis shows the formation of spherical $CaCO_3$ crystals (Fig. 1D) similar to those shown in Figs. 1A & B, indicating that the proteins secreted by *Verticillium* sp. into solution are responsible for the polymorph and morphology control and more importantly, that the growth of the crystals does not take place within specific reactions sites in the fungal biomass. The inset of Fig. 1D shows a higher magnification SEM image of spherical $CaCO_3$ crystals obtained, indicating that the crystallites in the control experiment are bigger (size ~500 nm) than those synthesized in the presence of the fungus (70–100 nm, Figs. 1A & B). The FTIR spectrum recorded from the crystals in the control experiment (Fig. 2D) exhibited absorption bands at 744 and 877 cm^{-1} which indicates formation of the vaterite polymorph (curve 3 in Fig. 2A). This occurs together with a weak absorption band at 712 cm^{-1}, that is characteristic of calcite.[16] XRD analysis of the $CaCO_3$ crystals in this control experiment also confirms the formation of vaterite (curve 3, Fig. 2B; peaks labeled by 'V') with evidence of a much smaller percentage of calcite (peaks labeled by 'C').[34] It is clear that the circular $CaCO_3$ crystallites are dominated by the vaterite polymorph. The presence of proteins in stabilizing the vaterite polymorph in the control experiment was detected by FTIR measurements (curve 3 in the inset of Fig. 2A) which shows the amide I and II bands and EDAX results show that the presence of strong N and S signals together with Ca, C and O signals (curve 3, Fig. 3A). We did not find any evidence for $CaCO_3$ growth on the fungal biomass.

The above experiments, particularly the control experiment involving proteins secreted by the fungus, clearly establish the important role played by the proteins in dictating morphology and polymorph control in $CaCO_3$ synthesis. The fact that the fungus also acts as a source of CO_2 makes this a truly biogenic method for the synthesis of minerals and is thus not merely biomimetic. That a non-calcareous microorganism such as a fungus should be capable of crystal growth and engineering at a high level of sophistication opens up the exciting possibility that other microorganisms when challenged with metal ions may lead to similar if not more exciting results. With this in mind, an actinomycete, *Thermomonospora* sp. isolated from self-heating compost was tested for $CaCO_3$ crystal growth in a manner similar to that carried out with *Verticillium* sp. Actinomycetes are microorganisms that share important characteristics of fungi and prokaryotes such as bacteria.[42] Even though they are classified as prokaryotes due to their close affinity with mycobacteria and the coryneforms (and thus amenable to genetic manipulation by modern recombinant DNA techniques), they were originally designated as "Ray Fungi" (Strahlenpilze). Focus on actinomycetes has primarily centered on their phenomenal ability to produce secondary metabolites such as antibiotics.[43] We have enlarged the scope of our studies and have identified the alkalothermophilic (extremophilic) actinomycete *Thermomonospora* sp.[44] as an exciting candidate for the biosynthesis of minerals. Unlike the case of *Verticillium* sp., *Thermomonospora* sp. upon reaction with aqueous Ca^{2+} ions resulted in the formation of $CaCO_3$ crystals both extracellularly and on the mycelia of the biomass. Figs. 4A–C show representative SEM images of extracellularly grown $CaCO_3$ crystals after reaction of aqueous Ca^{2+} ions with *Thermomonospora* sp. for 3 days. The $CaCO_3$ crystals in this case exhibit a morphology completely different from those biosynthesized using the fungus, *Verticillium* sp. (compare with Figs. 1A & B). A large number of plate-shaped crystals of $CaCO_3$ are observed which are organized in a composite superstructure (Figs. 4A & B). Viewed at higher magnification (Fig. 4C), the $CaCO_3$ plates appear to be quite uniform in thickness with smooth surfaces that are stacked on top of each other (Fig. 4C). The thickness of the $CaCO_3$ plates is calculated from the SEM images to be in the range 20–30 nm. Composite inorganic materials created by biological organisms from calcium salts and proteins are known to be architecturally complex and functionally diverse. These composites are known to provide superior mechanical stability in biological systems.[45] Such a bricks and mortar structure for composite crystals is known to occur in biominerals such as aragonite in gastropod nacre.[15] The bricks are flat crystals of $CaCO_3$ whereas the mortar is composed of biomacromolecules such as hydrophobic proteins and chitin.[14,15] These hybrid structures are known to have high mechanical strength and unusual optical properties.

The FTIR spectrum recorded from the *Thermomonospora* sp.-biogenic $CaCO_3$ composite crystals (Figs. 4A–C) is shown in Fig. 5A, curve 1. Three absorption bands are observed at 712, 856 and 874 cm^{-1} that provide evidence of the formation of a mixed phase of calcite (712 and 874 cm^{-1}) and aragonite (856 cm^{-1}).[46] The XRD pattern recorded from the $CaCO_3$ composite crystals is shown as curve 1 in Fig. 5B. It is observed that the $CaCO_3$ composite crystals consist of a mixed phase of the aragonite and calcite (reflections identified by 'A' for aragonite and 'C' for calcite) in agreement with the FTIR results. The EDAX spectrum recorded from the *Thermomonospora* sp.-biogenic $CaCO_3$ composite crystals is shown in Fig. 3B, curve 1. In addition to Ca, C and O signals, strong N and S signals are observed in this case as well indicating the presence of proteins within the composite plate-like crystals. The presence of proteins in the *Thermomonospora* sp.-biogenic $CaCO_3$ crystals is also indicated in the FTIR spectrum from this sample (curve 1, inset of Fig. 5A) where prominent amide I and II bands from the proteins are seen.

Figs. 4D–F show representative SEM images of $CaCO_3$ crystals that were growing on the surface of the actinomycete biomass (residue) after 3 days of reaction of aqueous Ca^{2+} ions with *Thermomonospora* sp. It is observed that the $CaCO_3$ crystals grow radially outward from the biomass surface in the form of highly elongated flat plates. The nature of the $CaCO_3$ crystals growing on the biomass is rather similar to those synthesized extracellularly (Figs. 4A–C) – the crystals are essentially in the form of flat plates that are then assembled into close-packed superstructures. One significant difference is observed, and that concerns the in-plane dimensions of the $CaCO_3$ plates. While the in-plane dimensions of the crystals are quite large in the case of extracellular growth, the $CaCO_3$ crystals growing on the biomass are in the form of slender

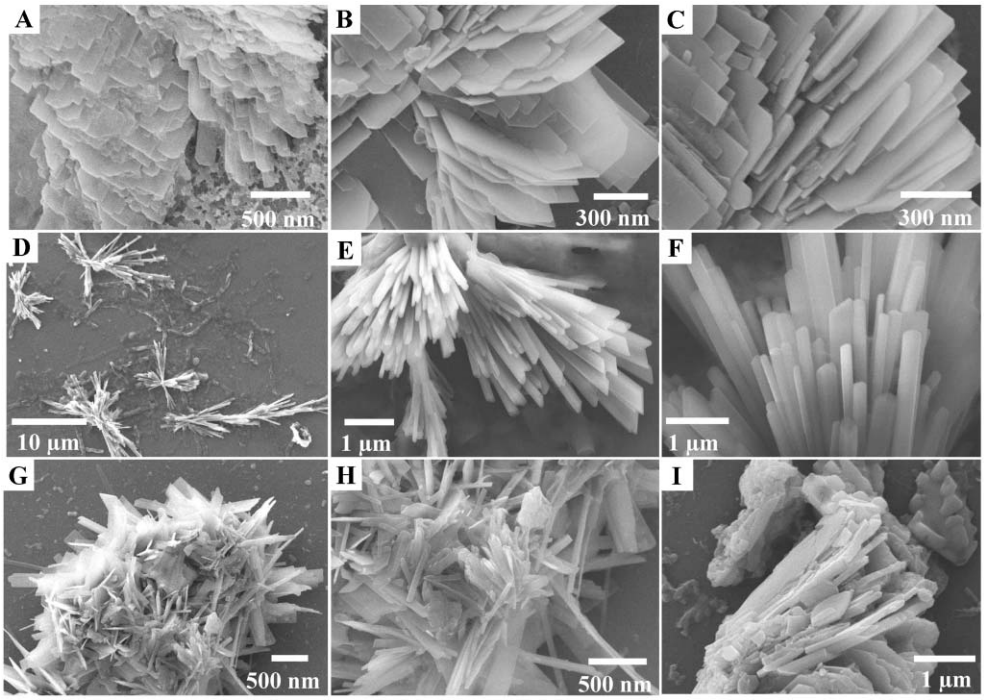

Fig. 4 (A–C) Representative SEM micrographs of extracellular $CaCO_3$ crystals after 3 days of reaction of aqueous Ca^{2+} ions with *Thermomonospora* sp. (D–F) SEM micrographs of intracellular $CaCO_3$ crystals after 3 days of reaction of aqueous Ca^{2+} ions with *Thermomonospora* sp. (G,H) SEM micrographs of extracellular $CaCO_3$ crystals (shown in A–C) after calcination at 300 °C for 3 h. (I) SEM micrograph of $CaCO_3$ crystals grown using extracts of *Thermomonospora* sp. (see text for details).

plates (Figs. 4D–F) that are much larger in length (5–15 μm) than in width (200–700 nm). The thickness of the $CaCO_3$ plates was measured to be 80–100 nm. While the exact reasons for the difference in behavior of the fungus and the actinomycete is not clear at the moment, *Thermomonospora* sp. appears to be capable of immobilizing Ca^{2+} ions on the surface, possibly through electrostatic interactions with the mycelial wall surface. Reaction of these entrapped ions with CO_2 released by the actinomycete could then lead to the formation of seed crystals on which secondary crystal growth could occur and thus formation of the elongated plate-like crystals. The anisotropy in the crystal shape and the assembly of the crystals observed could be due to constrained growth of the crystals due to the presence of the biomass surface that would affect the diffusivity of Ca^{2+} and CO_3^{2-} ions to nascent nuclei. It is clear that such a constraint would not occur for growth in solution and this is mirrored by the larger crystals grown extracellularly (Figs. 4A–C).

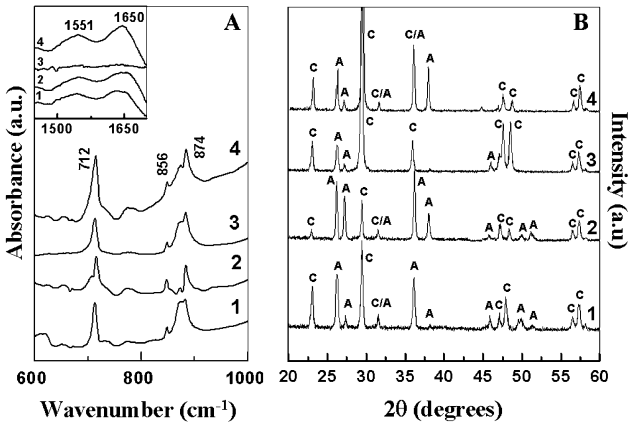

Fig. 5 (A and inset) FTIR spectra recorded in different spectral windows from $CaCO_3$ crystals synthesized extracellularly (curve 1) and on the biomass (curve 2) by the reaction of aqueous Ca^{2+} ions for 3 days with *Thermomonospora* sp.; the extracellularly synthesized sample after calcination at 300 °C for 3 h (curve 3) and FTIR spectrum recorded from $CaCO_3$ crystals grown using extract of *Thermomonospora* sp. (curve 4, text for details). (B) XRD patterns recorded from solution-cast films of $CaCO_3$ crystals synthesized extracellularly (curve 1) and on the biomass (curve 2) using *Thermomonospora* sp. on glass substrates and the extracellularly synthesized crystals after calcination at 300 °C for 3 h (curve 3). Curve 4 corresponds to the XRD pattern recorded from a solution-cast film of $CaCO_3$ crystals grown using extract from *Thermomonospora* sp. In the XRD spectra, 'A' stands for aragonite and 'C' for calcite (see text for details).

The FTIR spectrum recorded from the $CaCO_3$ crystals on the actinomycete biomass (Figs. D–F) is shown in Fig. 5A, curve 2. Absorption bands are observed at 712, 856 and 874 cm^{-1} in this case as well indicating the formation of a mixed phase of calcite and aragonite. The aragonite absorption bands (856 cm^{-1}, curve 2 in Fig. 5A) are enhanced relative to those observed with extracellularly synthesized $CaCO_3$ crystals (curve 1 in Fig. 5A). The XRD pattern provides clear support to the FTIR result showing that the percentage contribution of aragonite to the mixed phase with calcite is enhanced in the case of $CaCO_3$ grown on the *Thermomonospora* sp. biomass (curve 2 in Fig. 5B). The presence of proteins in the elongated $CaCO_3$ plates was determined by EDAX (curve 2 in Fig. 3B, N and S signals) and FTIR (curve 2 in the inset of Fig. 5A, strong amide I and II signatures) measurements.

To remove occluded proteins from the $CaCO_3$ composites grown using *Thermomonospora* sp., the protein–$CaCO_3$ composite crystals were calcined at 300 °C for 3 h. Figs. 4G & H show SEM images of the extracellularly synthesized $CaCO_3$ crystals after calcination. It is observed that, upon protein removal by calcination, the originally compact $CaCO_3$ plates collapse with no semblance of the original organized structure (Fig. 4G). The higher magnification SEM image (Fig. 4H) shows that the $CaCO_3$ plates have further disintegrated into smaller plates/needles. However, on a gross level the $CaCO_3$ crystallites have maintained their overall flat plate-like morphology after calcination. FTIR (curve 3 in Fig. 5A) and XRD (curve 3 in Fig. 5B) measurements of the calcined $CaCO_3$ samples still show the presence of a mixed calcite and aragonite phase with an increase in the percentage of calcite in the calcined crystals. The spot-profile EDAX spectrum

recorded from the calcined $CaCO_3$ crystals is shown as curve 3 in Fig. 3B. The complete disappearance of N and S signals from the EDAX spectrum indicates removal of proteins from the $CaCO_3$ composites, which is backed by the absence of amide bands in the FTIR spectrum shown as curve 3 in the inset of Fig. 5A.

A control experiment was performed in this case as well wherein the *Thermomonospora* sp. biomass was soaked in water for 3 days and the filtrate reacted with $CaCl_2$ and thereafter bubbled with CO_2 gas. The SEM image of $CaCO_3$ crystals formed in this manner is shown in Fig. 4I. This picture clearly shows the formation of flat $CaCO_3$ plates assembled into a superstructure rather similar to that observed for the crystals grown extracellularly during direct exposure to the actinomycete (Fig. 4C). The FTIR (curve 4 in Fig. 5A) and XRD (curve 4 in Fig. 5B) measurements revealed the formation of a mixed phase of aragonite and calcite. The presence of proteins in the $CaCO_3$ crystals in the control experiment was ascertained from EDAX (curve 4 in Fig. 3B, S and N signals) and FTIR measurements (curve 4 in the inset of Fig. 5A, strong amide bands).

The above experiments clearly indicate that the proteins secreted by the *Verticillium* sp. and *Thermomonospora* sp. are significantly different and capable of not only crystal morphology control but also polymorph selectivity. This is an important result with exciting implications for crystal engineering using biological systems. We believe the growth of the crystals proceeds in the following manner. In the first step, the Ca^{2+} ions (in the form of counterions) complex with the proteins secreted by the microorganisms leading to the formation of stable aggregates in solution. The entrapped Ca^{2+} ions then react with CO_2 *in situ* thereby forming $CaCO_3$ crystals in the mosaic structure inferred from FTIR and spot-profile EDAX analysis. This would explain the large concentration of proteins occluded in the crystals and provide a basis for understanding the morphology and polymorph control. On a more fundamental level, a clearer understanding of the mode of binding of specific proteins secreted by the microorganisms with different exposed faces of the crystals, the nature of the proteins (molecular weight, isoelectric point and possibly amino acid sequence as well) *etc.* would be important and is currently being pursued in this laboratory. Clearly, the use of proteins from non-calcareous microorganisms in crystal engineering is a new concept with much potential for development.

In order to understand whether the repeated washing of the biogenic $CaCO_3$ crystals synthesized using *Verticillium* sp. and *Thermomonospora* sp. results in the partial dissolution of the crystals or surface rearrangement in the minerals, the biogenic $CaCO_3$ crystals filtered from the respective culture media (without further washing) were analyzed by FTIR and SEM. Figs. 6A and C show SEM images recorded from the biogenic $CaCO_3$ crystals synthesized using *Verticillium* sp. and *Thermomonospora* sp. respectively under the above conditions. It is observed that the washing procedure does not lead to a significant structural and morphological change (compare Fig. 6A with Fig. 1A and Fig. 6C with Fig. 4C). We believe the washing process was successful in removing only free uncoordinated proteins present in the reaction medium and thus does not have any effect on the nature of the crystals formed.

In order to locate the large amount of proteins which are either deposited on the surface of the crystals or intercalated within the crystals, the solution containing biogenic $CaCO_3$ crystals were treated with 4% sodium hypochlorite (NaOCl) solution to remove any surface adsorbed proteins while preserving the proteins within the crystals. NaOCl treatment is known to be an efficient method to denature surface bound proteins due to its oxidizing capability. Figs. 6B and D show

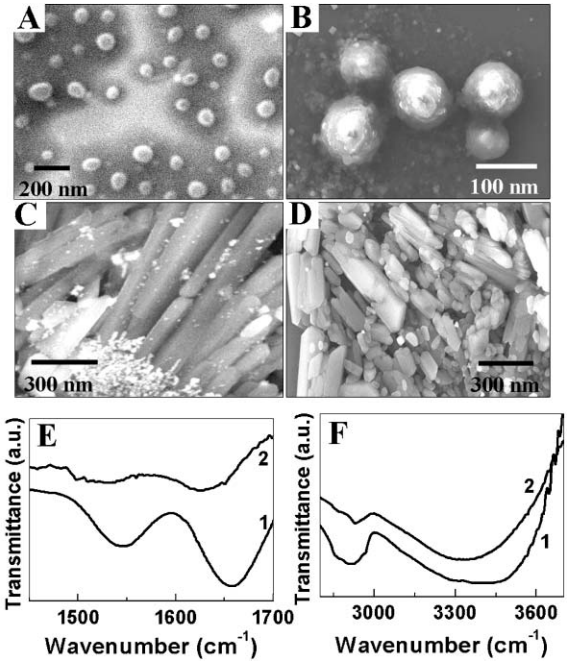

Fig. 6 (A and B) Representative SEM micrographs of $CaCO_3$ crystals grown after 3 days of reaction of aqueous Ca^{2+} ions with *Verticillium* sp. before (A) and after (B) treatment with NaOCl solution. (C and D) Representative SEM micrographs of $CaCO_3$ crystals grown after 3 days of reaction of aqueous Ca^{2+} ions with *Thermomonospora* sp. before (C) and after (D) treatment with NaOCl solution. (E and F) FTIR spectra in different spectral windows recorded from: $CaCO_3$ crystals obtained by the reaction of aqueous Ca^{2+} ions for 3 days with *Thermomonospora* sp. before (curve 1) and after treatment with NaOCl solution (curve 2) (see text for details).

SEM images recorded from solution-cast films of the biogenic $CaCO_3$ crystals synthesized using *Verticillium* sp. and *Thermomonospora* sp. respectively after NaOCl treatment. On the spherical vaterite crystals (Fig. 6A, obtained using *Verticillium* sp.), nucleation of secondary crystallites is observed which indicates partial dissolution of vaterite crystals (Fig. 6B) upon NaOCl treatment and the recrystallization to the more stable calcite polymorph (as evidenced from FTIR results, data not shown). Similarly, NaOCl treatment of $CaCO_3$ crystals synthesized using *Thermomonospora* sp. leads to the collapse of originally organized $CaCO_3$ plate-composites (Fig. 6C) into smaller individual plates (Fig. 6D). This suggests that most of the proteins which were present on the surface of the crystalline framework have been removed upon addition of NaOCl and contribute to the change in the crystal structure and morphology described above. FTIR spectra were recorded from the biogenic $CaCO_3$ crystals synthesized using *Thermomonospora* sp. before (curve 1 in Fig. 6E) and after (curve 2 in Fig. 6E) NaOCl treatment. The amide bands in the FTIR spectrum (curve 1 in Fig. 6E) indicate the presence of protein in the $CaCO_3$ crystals. Removal of large amounts of proteins from the biogenic $CaCO_3$ crystals upon NaOCl treatment is evidenced from the FTIR measurement (curve 2 in Fig. 6E), which clearly shows that the amide bands are reduced considerably in intensity. It is also possible that other soluble biomacromolecules/molecules such as polysaccharides secreted by the cells may have contributed to $CaCO_3$ morphology and control observed in reactions using the fungus and actinomycete. The presence of a strong –OH band in the FTIR spectrum obtained from $CaCO_3$ crystals, synthesized using *Thermomonospora* sp. before (curve 1 in Fig. 6F) and after (curve 2 in Fig. 6F) NaOCl treatment, may be attributed to the presence of polysaccharides released by the microorganisms during formation of the $CaCO_3$ crystals. While some loss in overall structure of the vaterite and calcite assemblies is observed

during removal of surface-bound protein by NaOCl treatment (Figs. 6B and D), indicating that proteins play an important role in directing the morphology and crystallography of the minerals, the role of polysaccharides and other biomolecules is yet to be fully understood.

To demonstrate the generality of this method for the biosynthesis of minerals, we have also examined the synthesis of another important metal carbonate, $BaCO_3$ with *Verticillium* sp. and *Thermomonospora* sp. by reaction of aqueous Ba^{2+} ions with the biomass. Figs. 7A & B correspond to representative SEM images recorded from solution-cast films of the aqueous $BaCl_2$ solution after exposure to *Verticillium* sp. for 2 days. The formation of spheroidal $BaCO_3$ particles along with needle like structures is observed in this experiment. The formation of $BaCO_3$ in a needle-like morphology is known to commonly occur in solution whereas the formation of spheroidal $BaCO_3$ is possibly mediated by proteins secreted from the fungus. The higher magnification SEM image (Fig. 7B) clearly shows the $BaCO_3$ spheroids in greater detail. The size of the $BaCO_3$ spheroids are calculated to be in the range of 200–500 nm. The surface of the spheres is highly irregular and they appear to be composed of smaller crystallites. The XRD pattern recorded from the $BaCO_3$ spheroids is shown as curve 1 in Fig. 8. A number of Bragg reflections are identified and have been indexed with reference to the unit cell of the Witherite structure of $BaCO_3$ (orthorhombic structure with cell constants $a = 5.315$ Å, $b = 8.904$ Å, $c = 6.433$ Å and space group *Pnma*).[47] The spot-profile EDAX measurement of one of the spherical $BaCO_3$ crystals yielded Ba, C and O signals close to the expected stoichiometric values along with the presence of N and S signals that are indicative of the presence of proteins within the spherical $BaCO_3$ superstructures (data not shown). It is observed that the $BaCO_3$ spheroids consist of nanosized subunits in the form of needles. It is quite possible that the nanosized precursors (needles) are formed initially and act as nucleating agents for the subsequent growth/aggregation into spheroids and stabilization by protein. $BaCO_3$ in a spheroidal morphology has previously been observed in the presence of double hydrophilic block copolymers as a template.[31] Matijevic *et al*. have observed similar spheroidal morphology for $BaCO_3$ and $SrCO_3$ crystals synthesized by the enzyme-catalyzed decomposition of urea by urease at low temperatures.[30] To remove occluded proteins from the $BaCO_3$ spheroids grown using *Verticillium* sp., the protein–$BaCO_3$ composite crystals were calcined at 300 °C for 3 h. Fig. 7C shows an SEM image of calcined biogenic $BaCO_3$ spheroids. It is observed that, upon protein removal, the originally compact

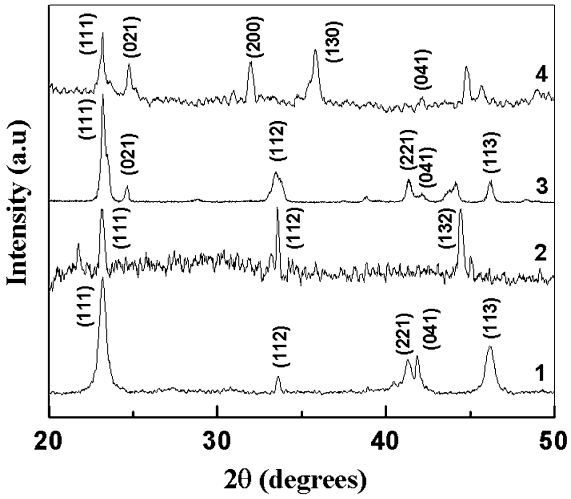

Fig. 8 XRD patterns recorded from solution-cast films of $BaCO_3$ crystals synthesized using *Verticillium* sp. on glass substrate before (curve 1) and after calcination at 300 °C for 3 h (curve 2). XRD patterns recorded from solution-cast films of $BaCO_3$ crystals synthesized using *Thermomonospora* sp. on glass substrate before (curve 3) and after calcination at 300 °C for 3 h (curve 4). The Bragg reflections are identified in all spectra.

$BaCO_3$ spheroids collapse into a disordered structure. The XRD measurement from the calcined $BaCO_3$ spheroids is shown as curve 2 in Fig. 8. The reduction in the (111) Bragg reflection, along with the disappearance of some of the other Bragg reflections, clearly indicates that protein removal from $BaCO_3$ spheroids leads to some internal restructuring in the composite $BaCO_3$ crystals.

Figs. 7D & E correspond to representative SEM images recorded from solution-cast films of the aqueous $BaCl_2$ solution after exposure to *Thermomonospora* sp. for 2 days. The lower magnification SEM image (Fig. 7D) shows the formation of small $BaCO_3$ crystallites assembled into a branched structure. At higher magnification (Fig. 7E), the quasi-linear structures are seen to be composed of individual plate-like $BaCO_3$ crystallites. The size of these individual $BaCO_3$ plates is calculated to be in the range of 100–500 nm. As in the case of $CaCO_3$ synthesis using the fungus and the actinomycete where significant differences in the crystal morphology (and indeed, crystal structure) were observed, we observe large differences in the $BaCO_3$ crystal morphology as well underlining the extremely important role played by the

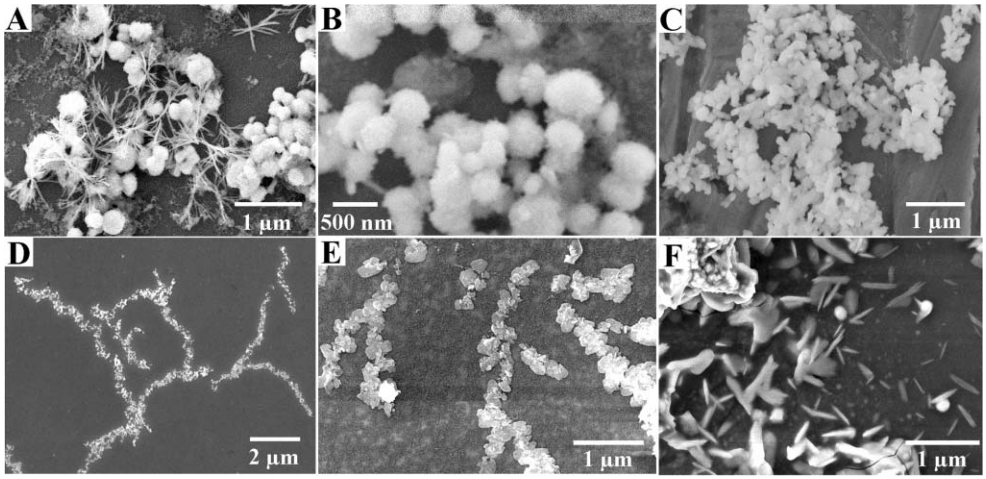

Fig. 7 (A and B) Representative SEM micrographs of $BaCO_3$ crystals after 2 days of reaction of aqueous Ba^{2+} ions with *Verticillium* sp. (C) SEM micrograph of $BaCO_3$ crystals (shown in A and B) after calcination at 300 °C for 3 h. (D and E) SEM micrographs of $BaCO_3$ crystals after 2 days of reaction of aqueous Ba^{2+} ions with *Thermomonospora* sp. (F) SEM micrograph of $BaCO_3$ crystals (shown in D and E) after calcination at 300 °C for 3 h.

proteins secreted by these two microorganisms in morphology and crystal structure control. The XRD pattern recorded from these $BaCO_3$ assemblies is shown as curve 3 in Fig. 8. The Bragg reflections in the XRD spectrum are identified and have been indexed with reference to the unit cell of the Witherite structure of $BaCO_3$.[47] EDAX and FTIR measurements from these $BaCO_3$ assemblies indicated the presence of occluded proteins. Calcination was induced to remove proteins from the $BaCO_3$–protein composites and resulted in the formation of individual $BaCO_3$ platelets (Fig. 7F). The XRD measurements from the calcined $BaCO_3$ crystals (Fig. 8, curve 4) show some changes in the relative intensities of the Bragg reflections that could still be indexed based on the Witherite structure. This indicates substantial restructuring of the composite crystals further to protein removal and some oriented assembly of the crystallites.

The difference in morphology of the $CaCO_3$ and $BaCO_3$ crystals synthesized using a fungus, *Verticillium* sp. and an actinomycete, *Thermomonospora* sp. is interesting and may be attributed to the different proteins secreted by these microorganisms. Further work is required to determine the nature of these proteins, how they bind to the $CaCO_3$ and $BaCO_3$ crystallographic faces and also how they modulate the diffusivity of the constituent ions to the surface of growing crystallites in solution. The formation of spherical and flat plate-like $CaCO_3$ and $BaCO_3$ crystals by the reaction of aqueous Ca^{2+} and Ba^{2+} ions with a fungus, *Verticillium* sp. and an actinomycete, *Thermomonospora* sp. indicates that specific proteins secreted by these organisms are responsible for the shape and polymorph control of $CaCO_3$ and $BaCO_3$ crystals.

In conclusion, the total biological synthesis of $CaCO_3$ and $BaCO_3$ crystals of interesting morphology and polymorph selectivity by challenging microorganisms such as a fungus and an actinomycete with aqueous Ca^{2+} and Ba^{2+} ions respectively has been described. We term this process 'total biosynthesis' since the source of carbonate ions is the microorganisms themselves and is thus at variance with other biomimetic methods wherein an external source of CO_2 was used to grow the minerals. Through reaction of the metal ions with the two microorganisms, we have shown that specific proteins secreted by the microorganisms play a very important role in directing the morphology and crystal structure of the minerals grown in solution. Our finding that minerals of such complex morphology can be grown by a completely biological process using microorganisms that are not normally (if ever) exposed to such metal ions is exciting with important implications in crystal engineering and associated applications. From the point of view of scale-up of production of minerals, the use of a renewable source of CO_2 and crystal-modifying proteins from microorganisms is obvious.

Acknowledgements

DR thanks the Department of Science and Technology (DST), Government of India for a research fellowship. We acknowledge the SEM/EDAX and XRD facilities of the Center for Materials Characterization, NCL Pune.

References

1 A. Berman, J. Hanson, L. Leiserowitz, T. F. Koetzle, S. Weiner and L. Addadi, *Science*, 1993, **259**, 776.
2 S. Weiner and L. Addadi, *J. Mater. Chem.*, 1997, **7**, 689.
3 K. Simkiss and K. Wilbur, *Biomineralization*, Academic Press, New York, 1989.
4 S. Mann, *Biomimetic Materials Chemistry*. John Wiley & Sons Publishers, Weinheim, 1995.
5 D. R. Loveley, J. F. Stolz, G. L. Nord and E. J. P. Phillips, *Nature*, 1987, **330**, 252.
6 H. Spring and K. H. Schleifer, *Syst. Appl. Microbiol.*, 1995, **18**, 147.
7 D. P. E. Dickson, *J. Magn. Mater.*, 1999, **203**, 46.
8 S. Mann, *Nature*, 1993, **365**, 499.
9 S. Oliver, A. Kupermann, N. Coombs, A. Lough and G. A. Ozin, *Nature*, 1995, **378**, 47.
10 N. Kroger, R. Deutzmann and M. Sumper, *Science*, 1999, **286**, 1129.
11 D. Pum and U. B. Sleytr, *Trends Biotechnol.*, 1999, **17**, 8.
12 U. B. Sleytr, P. Messner, D. Pum and M. Sara, *Angew. Chem., Int. Ed.*, 1999, **38**, 1034.
13 R. Lakshminarayanan, R. M. Kini and S. Valiyaveettil, *Proc. Natl. Acad. Sci. USA*, 2002, **99**, 5155.
14 T. Kato, A. Sugawara and N. Hosoda, *Adv. Mater.*, 2002, **14**, 869.
15 C. M. Zaremba, D. E. Morse, S. Mann, P. K. Hansma and G. D. Stucky, *Chem. Mater.*, 1998, **10**, 3813.
16 G. Falini, S. Albeck, S. Weiner and L. Addadi, *Science*, 1996, **271**, 67.
17 B. R. Heywood and S. Mann, *Adv. Mater.*, 1994, **6**, 9.
18 S. Rajam, B. R. Heywood, J. B. A. Walker and S. Mann, *J. Chem. Soc., Faraday Trans.*, 1991, **87**, 727.
19 B. R. Heywood, S. Rajam and S. Mann, *J. Chem. Soc., Faraday Trans.*, 1991, **87**, 735.
20 S. Mann, B. R. Heywood, S. Rajam and J. D. Birchall, *Nature*, 1988, **334**, 692.
21 E. Loste, E. D. Marti, A. Zarbakhsh and F. C. Meldrum, *Langmuir*, 2003, **19**, 2830.
22 D. Rautaray, A. Banpurkar, S. R. Sainkar, A. V. Limaye, N. R. Pavaskar, S. B. Ogale and M. Sastry, *Adv. Mater.*, 2003, **15**, 1273.
23 J. Kuther, G. Nelles, R. Seshadri, M. Schaub, H.-J. Butt and W. Tremel, *Chem. Eur. J.*, 1998, **4**, 1834.
24 C. Damle, A. Kumar, M. Bhagwat, S. R. Sainkar and M. Sastry, *Langmuir*, 2002, **18**, 6075.
25 D. Walsh and S. Mann, *Nature*, 1995, **377**, 320.
26 J. Aizenberg, D. A. Muller, J. L. Grazul and D. R. Hamman, *Science*, 2003, **299**, 1205.
27 L. Qi, J. Li and J. Ma, *Adv. Mater.*, 2002, **14**, 300.
28 J. J. J. M. Jonners, R. J. M. Nolte and N. A. J. M. Sommerdijk, *J. Am. Chem. Soc.*, 2002, **124**, 9700.
29 S. H. Yu, H. Colfen, A. W. Xu and W. Dong, *Cryst. Growth Des.*, 2004, **4**, 33.
30 I. Sondi and E. Matijevic, *Chem. Mater.*, 2003, **15**, 1322.
31 S. H. Yu, H. Colfen and M. Antonietti, *J. Phys. Chem. B*, 2003, **107**, 7396.
32 C. Couriol, A. Amrane and Y. Progent, *J. Biosci. Bioeng.*, 2001, **91**, 570.
33 D. Rautaray, A. Ahmad and M. Sastry, *J. Am. Chem. Soc.*, 2003, **125**, 14656.
34 N. Nassrallah-Aboukais, A. Boughriet, J. Laureyns, A. Aboukais, J. C. Fischer, H. R. Langelin and M. Wartel, *Chem. Mater.*, 1998, **10**, 238.
35 L. Brecevic, V. Nothing-Laslo, D. Kralji and S. Popovic, *J. Chem. Soc., Faraday Trans.*, 1996, **92**, 1017.
36 A. Lopezmacipe, J. Gomezmorales and R. Rodriguezclemente, *J. Cryst. Growth*, 1996, **166**, 1015.
37 J. M. Didymus, P. Oliver, S. Mann, A. L. Devries, P. V. Hauschka and P. Westbroek, *J. Chem. Soc., Faraday Trans.*, 1993, **89**, 2891.
38 H. Colfen and M. Antonietti, *Langmuir*, 1998, **14**, 582.
39 H. Colfen and L. Qi, *Chem. Eur. J.*, 2001, **7**, 106.
40 K. Naka, Y. Tanaka and Y. Chujo, *Langmuir*, 2002, **18**, 3655.
41 I. Sondi and E. Matijevic, *J. Colloid Interface Sci.*, 2001, **238**, 208.
42 Y. Okami, T. Beppu and H. Ogawara, *Biology of Actinomycetes*, Japan Scientific Societies Press, Tokyo, 1988, p. 508.
43 T. Sasaki, J. Yoshida, M. Itoh, S. Gomi, T. Shomura and M. Sezaki, *J. Antibiot.*, 1988, **41**, 835.
44 Extremophiles are microorganisms that thrive under conditions that are lethal to human beings, such as extremes of temperature [from −14 °C (psychrophiles) to 45 °C (thermophiles) to 110 °C (hyperthermophiles)]; extremes of pH [from 1 (acidophiles) to 9 (alkalophiles)]; very high barostatic pressure (barophiles); non-aqueous environments containing 100% organic solvents, excess heavy metal concentration *etc*. These microorganisms have developed numerous special adaptations to survive in such extreme habitats, which include new mechanisms of energy transduction, regulating intracellular environment and metabolism, maintaining the structure and functioning of membrane and enzymes, *etc*.
45 L. Addadi and S. Weiner, *Nature*, 1997, **389**, 912.
46 L. Wang, I. Sondi and E. Matijevic, *J. Colloid Interface Sci.*, 1999, **218**, 545.
47 The XRD patterns were indexed with reference to the unit cell of the witherite structure of $BaCO_3$ from *ASTM* chart (a = 5.315 Å, b = 8.904 Å, c = 6.433 Å; space group *Pnma*, ASTM chart card no. 5-0378).